^{19}Mg two-proton decay lifetime

P. Voss,[1,2,3,*] T. Baumann,[2] D. Bazin,[2] A. Dewald,[4] H. Iwasaki,[1,2] D. Miller,[1,2,†] A. Ratkiewicz,[1,2,‡] A. Spyrou,[1,2] K. Starosta,[3] M. Thoennessen,[1,2] C. Vaman,[2] and J. A. Tostevin[5]

[1]*Department of Physics and Astronomy, Michigan State University, East Lansing, Michigan 48824, USA*
[2]*National Superconducting Cyclotron Laboratory, East Lansing, Michigan 48824, USA*
[3]*Department of Chemistry, Simon Fraser University, Burnaby, British Columbia V5A 1S6, Canada*
[4]*Institut für Kernphysik, Universität zu Köln, 50937 Köln, Germany*
[5]*Department of Physics, University of Surrey, Guildford GU2 7XH, United Kingdom*

(Received 5 May 2014; published 8 July 2014)

The ground state two-proton decay lifetime of ^{19}Mg, populated by the one-neutron knockout of an intermediate-energy ^{20}Mg radioactive beam, was measured utilizing a new experimental technique. A thin silicon detector positioned at varying distances (0.0–1.0 mm) downstream of the reaction target measured the energy loss of ^{19}Mg and the two-proton decay product ^{17}Ne. The lifetime was deduced from fits to the measured energy-loss line shapes and depended upon the contribution of prompt reaction processes to the yield of ^{17}Ne. For relative ^{17}Ne prompt contributions from 82% to 92%, the extracted lifetimes ranged from $1.75^{+0.43}_{-0.42}$ to $6.4^{+2.4}_{-2.7}$ ps. The results are consistent with the previously reported ^{19}Mg lifetime measurement and serve as both an important complementary study and a validation of this new technique, which can provide lifetime information for short-lived states beyond the proton drip line.

DOI: 10.1103/PhysRevC.90.014301 PACS number(s): 23.50.+z, 21.10.Tg, 27.20.+n, 29.30.Ep

I. INTRODUCTION

Mapping the limits of nuclear existence and performing precise spectroscopy of rare atomic nuclei with extreme proton-neutron asymmetries requires the development of sensitive experimental techniques to surmount short lifetimes, low production cross sections, and large background signals. The exotic two-proton ($2p$) decay of even-Z nuclei beyond the proton drip line exemplifies such challenges; more than 40 years passed between prediction [1] and experimental confirmation [2,3].

Lifetime measurements have proven to be an important probe of the decay properties of these short-lived $2p$-emitting nuclei. For example, the $2p$-emission lifetimes of ^{45}Fe [2–5], ^{48}Ni [4,6], and ^{54}Zn [7] have been measured to be several milliseconds. In comparison with theoretical predictions, these relatively long lifetimes provided strong evidence for the necessity of a three-body quantum mechanical description of the decay process; modeling the decay as the tunneling of a diproton (^{2}He nucleus) typically yielded lifetimes several orders of magnitude too short (cf. Refs. [8–10]). Subsequently, direct visual evidence in support of a true three-body decay was observed in ^{45}Fe [5] and ^{48}Ni [6] using the optical time-projection chamber technique. For lighter nuclei, both the Coulomb and the centrifugal barriers are reduced with respect to the aforementioned, medium-mass $2p$ emitters, and the lifetimes are correspondingly shorter. Therefore, to access the wealth of nuclear structure information beyond the proton drip line, a wide variety of experimental techniques are required.

In this work, we present an adaptation of the well-established recoil distance method used in γ-ray spectroscopy [11] for lifetime measurements of proton emitters with lifetimes from 10^{-13} to 10^{-10} s. The $2p$ emitter ^{19}Mg was chosen for the first application of this new technique. The ground state $2p$-decay mean lifetime was previously measured to be $\tau = 5.8 \pm 2.2$ ps ($T_{1/2} = 4.0 \pm 1.5$ ps) via trajectory reconstruction of all three decay components ($^{17}\mathrm{Ne} + p + p$) [12]. The results fell well within the predicted 0.5 to 60 ps lifetime range of a three-body decay calculation [13] and near the upper limit of the 0.06 to 8.2 ps lifetime range assuming a diproton emission model [14,15]. Both models favored a dominant d^2 configuration for the ^{19}Mg valence protons. However, spectroscopy of the unbound intermediary nucleus ^{18}Na uncovered unexpected low-lying broad s-wave resonances; ^{19}Mg lifetime estimates via sequential $1p$ decays through these states were as low as 1 ps [16].

This wide range of predicted lifetimes warrants an independent confirmation of the measured results using a new and complementary method. Hence, a particle plunger variant of the Köln/NSCL plunger [17] for lifetime measurements beyond the proton drip line was developed. In this technique, a double-sided silicon strip detector (DSSD) is installed in place of the plunger degrader to measure the energy loss of reaction and decay residues (^{19}Mg and ^{17}Ne, respectively) emerging from the target in coincidence with ion identification in the S800 Magnetic Spectrograph [18]. Lifetime information can then be extracted from the variation of ^{19}Mg and ^{17}Ne energy-loss peak intensities at various target-DSSD distances.

II. EXPERIMENTAL METHOD

The lifetime measurement was performed at the National Superconducting Cyclotron Laboratory (NSCL). A 170 MeV/nucleon ^{24}Mg^{12+} primary beam was accelerated

*Correspondence author: pvoss@sfu.ca
†Present address: TRIUMF, 4004 Wesbrook Mall, Vancouver, BC V6T 2A3, Canada.
‡Present address: Department of Physics and Astronomy, Rutgers University, New Brunswick, New Jersey 08903, USA.

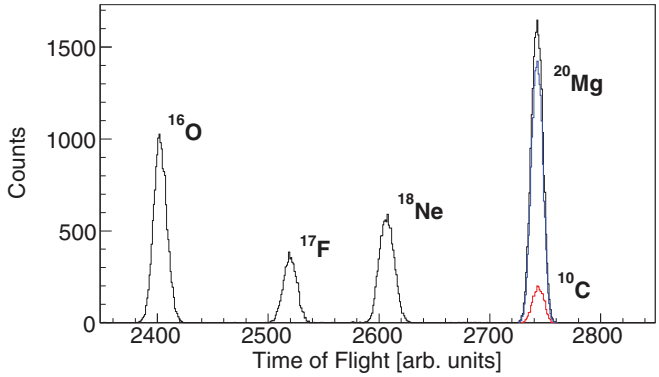

FIG. 1. (Color online) Identification of the secondary beam components by their time of flight between two thin plastic scintillators at the A1900 focal plane and the S800 object position. Energy-loss differences of ^{10}C (lower red line) and ^{20}Mg (upper blue line) in the S800 ionization chamber were used to separate the two components of the rightmost peak.

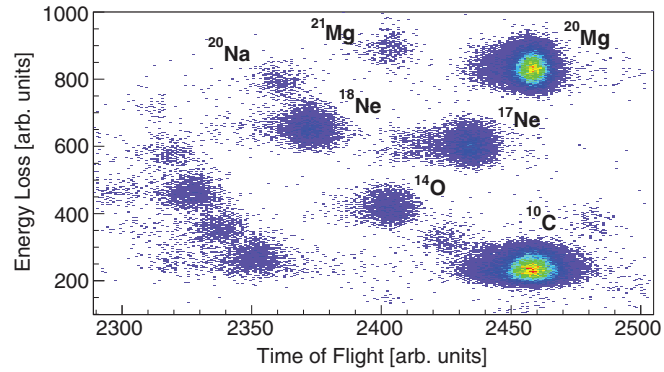

FIG. 2. (Color online) Outgoing reaction- and decay-residue identification from incoming ^{20}Mg by time of flight and energy-loss information from the S800 Spectrograph tuned for acceptance of ^{17}Ne^{10+}.

by the Coupled Cyclotron Facility and impinged upon a 1081 mg/cm^2 ^{9}Be production target. A radioactive ^{20}Mg secondary beam was selected from the fragmentation reaction products by the A1900 Fragment Separator [19]. Three significant beam contaminants—^{16}O (29%), ^{17}F (11%), and ^{18}Ne (19%)—were distinguished from ^{20}Mg (36%) by their time of flight between two thin plastic scintillators at the A1900 focal plane and the S800 object position, as illustrated in Fig. 1. The ^{10}C contaminant, with the same charge-to-mass ratio as ^{20}Mg (and hence the same time of flight), was separated by energy-loss differences in the S800 ionization chamber [20].

The ^{20}Mg secondary beam was delivered to the Köln/NSCL particle plunger at the S800 target position with an energy of 91 MeV/nucleon and an average intensity of 1600 pps. States in ^{19}Mg were populated via a one-neutron knockout reaction on a 110 mg/cm^2 (0.49 mm) ^{nat}C target and the nucleus decayed by $2p$ emission to ^{17}Ne after a flight distance governed by the lifetime and beam velocity. The energy-loss profile of each ion emerging from the target was detected in a 69 mg/cm^2 (0.30 mm) DSSD mounted perpendicular to the beam axis immediately downstream of the target. Knockout-reaction and decay residues were identified on an event-by-event basis by their energy loss in the S800 ionization chamber and time of flight between plastic scintillators at the S800 object position and focal plane as depicted in Fig. 2. DSSD energy-loss signals were recorded in coincidence with these residues to suppress background from contaminant reaction residues outside of the S800 momentum acceptance. For the lifetime analysis, events corresponding to the $^{19}\text{Mg} \rightarrow {}^{17}\text{Ne} + p + p$ decay channel were selected by an incoming ^{20}Mg time-of-flight gate and an outgoing ^{17}Ne particle gate at the S800 focal plane.

III. EXPERIMENTAL RESULTS

^{17}Ne-gated DSSD energy-loss spectra were collected at target-DSSD distances of 0.0, 0.1, 0.2, 0.5, and 1.0 mm. In addition to the delayed ground state $2p$ decay of ^{19}Mg, three indistinguishable prompt processes, occurring on a time scale ($t < \sim 10^{-15}$ s) well below our experimental sensitivity, contributed to the observed ^{17}Ne yield: the $2p1n$ breakup of the ^{20}Mg secondary beam, the $1p1n$ breakup followed by prompt proton emission from unbound ^{18}Na [16,21,22], and sequential $1p$ emissions of ^{19}Mg excited states through broad resonances in ^{18}Na. Furthermore, the ^{20}Mg beam had sufficient energy to pass unreacted through the target and undergo knockout reactions on the DSSD. Together, the combination of delayed and prompt ^{17}Ne production processes and reactions on both the target and the DSSD yielded the energy-loss line shape shown in Fig. 3(a). There, the prominent peak corresponds to neon energy loss—from the $2p$ decay of ^{19}Mg and the prompt production of ^{17}Ne, both in the target. The small enhancement at higher energy corresponds to magnesium energy loss—from the production of ^{19}Mg in the target or detector and $2p$ decay farther downstream. The broad plateau between these extremes corresponds to events with mixed neon and magnesium energy losses.

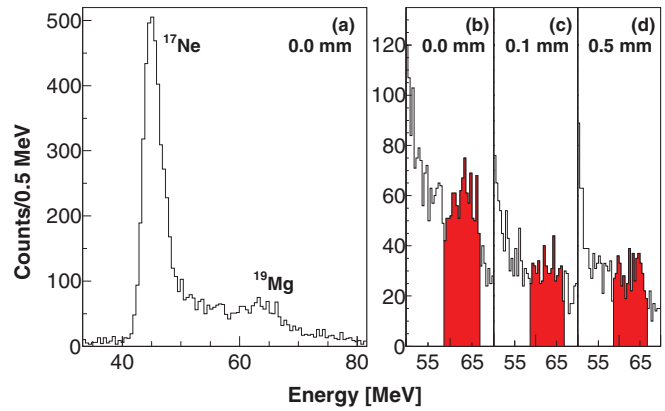

FIG. 3. (Color online) DSSD energy-loss spectra in coincidence with incoming ^{20}Mg on the target and outgoing ^{17}Ne in the S800. (a) The full spectrum for the 0.0 mm target-DSSD distance. (b–d) The region surrounding the ^{19}Mg energy-loss peaks (shaded red) for distances of 0.0 mm (b), 0.1 mm (c), and 0.5 mm (d).

IV. SIMULATIONS AND ANALYSIS

Fitting the DSSD energy-loss data with simulated line shapes generated with various input lifetimes and then applying a χ^2 goodness-of-fit test yields the best-fit lifetime. The DSSD line-shape simulations and statistical analysis were performed within the GEANT4 [23] and ROOT [24] toolkits and were modified from γ-ray line-shape simulation software used extensively for recoil distance method lifetime analyses [25–27]. Obtaining accurate energy-loss line shapes required a parametrization of the experimental details impacting the observed reaction- and decay-residue momentum distributions. In particular, the simulations accurately reproduced the S800 momentum acceptance and the DSSD detector response, as well as the ^{20}Mg secondary beam emittance, the knockout-reaction kinematics, and the subsequent energy and angular straggling of both ^{19}Mg and ^{17}Ne in the target and detector. Figure 4 illustrates the quality of select fits to the data.

DSSD energy-loss spectra in coincidence with incoming ^{20}Mg on the target and outgoing ^{18}Ne in the S800 (see Fig. 2) were used to properly account for the high-energy background extending beyond the ^{19}Mg energy-loss region evident in Fig. 3. These events originated from the $2p$ knockout of the ^{20}Mg secondary beam or the proton decay of the $1p$-knockout residue ^{19}Na. Shell model calculations of the proton-decay width indicate that the unbound ^{19}Na ground state has an approximately 1 fs decay lifetime [28]. Both processes contributing to these ^{18}Ne energy-loss line shapes are thus prompt, allowing the high-energy background to be parametrized without the presence of lifetime effects. The background parameters were determined from the simulated best-fit to the ^{18}Ne-gated energy-loss line shapes at a fixed lifetime of $\tau = 0$ ps and were subsequently applied to the ^{19}Mg analysis.

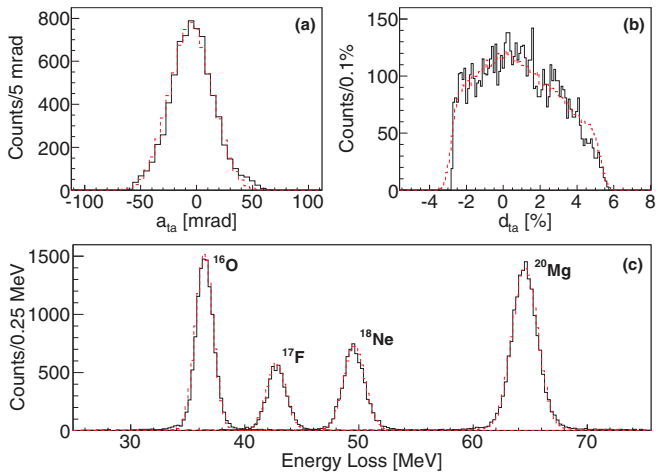

FIG. 4. (Color online) Fit of simulated (dashed red line) and experimental (solid black line) ^{17}Ne particle-gated S800 reaction residue spectra for (a) the angular spread in the energy-dispersed direction (a_{ta}) and (b) the kinetic energy deviation from that corresponding to a central trajectory through the S800 (d_{ta}). (c) Experimental (solid black line) and simulated (dashed red line) DSSD energy-loss line shapes for the four dominant unreacted secondary beam components.

The contribution of prompt processes to the observed ^{17}Ne yield was parametrized by a production mechanism ratio, R_p, given by

$$R_p = \frac{N_{\text{prompt}}}{N_{\text{delayed}} + N_{\text{prompt}}}. \quad (1)$$

Here, a value of 0 corresponds to 100% delayed production of ^{17}Ne by the $2p$ decay of the ^{19}Mg ground state and N_{prompt} is the sum of the three processes discussed above. Similarly, the ratio of knockout reactions on the target to those on the detector, R_σ, was parametrized as

$$R_\sigma = \frac{N_{\text{tar}}}{N_{\text{det}}}. \quad (2)$$

Therefore, with the simulation parameters systematically fixed to reproduce the observed momentum distributions and high-energy background, DSSD energy-loss line shapes were constructed within the three-dimensional parameter space of τ, R_p, and R_σ. We have performed knockout-reaction cross section calculations to constrain R_σ. Assuming p-wave neutron removal from ^{20}Mg at beam energies between 80 and 90 MeV/nucleon, we obtained a reaction ratio of $R_\sigma = 3.2$. Additional calculations using EPAX 2.15 [29] and Abration Ablation [30,31] fragmentation parametrizations within LISE++ [32] yielded ratios of $R_\sigma = 2.9$ and 3.3, respectively. Finally, similar LISE++ cross section estimates were obtained for the $1p$ knockout producing ^{19}Na, and the best-fit simulations of its subsequent prompt $1p$-decay data were obtained within the well-constrained range $R_\sigma = [3.0,3.4]$. We have therefore adopted the values $R_\sigma = 3.0$, 3.2, and 3.4 for the ^{19}Mg analysis.

In contrast, we have taken a twofold approach for the constraint of the ^{17}Ne production mechanism ratio. First, the ratio was left unconstrained and lifetimes were determined in 10% intervals within the range $R_p = [0.05,0.95]$. These results highlight the effect of an increasing ^{17}Ne prompt production on the best-fit $2p$-decay lifetime of ^{19}Mg; in general, larger values of R_p require longer lifetimes to properly fit the data. In addition, tighter constraints were placed on the ^{17}Ne production mechanism ratio in an effort to compare our results

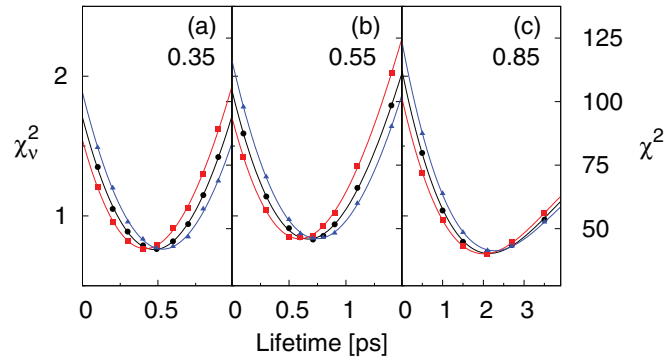

FIG. 5. (Color online) Distributions of χ^2 and χ^2_ν (reduced χ^2) values from the fits of simulations to the 0.0 mm energy-loss data for ^{17}Ne production mechanism ratios $R_p = 0.35$ (a), $R_p = 0.55$ (b), and $R_p = 0.85$ (c) and target-DSSD reaction ratios $R_\sigma = 3.0$ (red squares), $R_\sigma = 3.2$ (black circles), and $R_\sigma = 3.4$ (blue triangles).

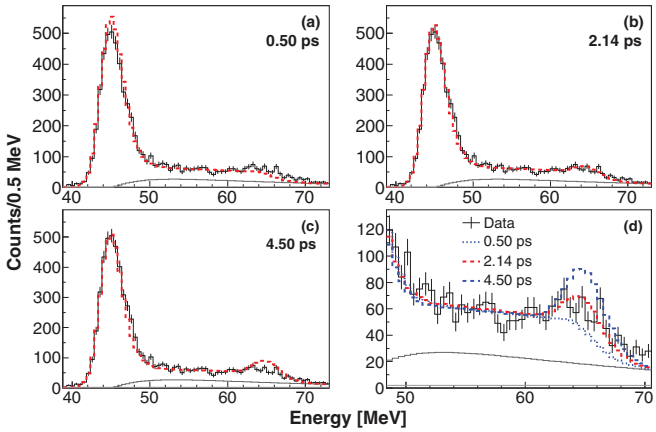

FIG. 6. (Color online) The 0.0 mm experimental DSSD spectra in coincidence with incoming ^{20}Mg on the target and outgoing ^{17}Ne in the S800 with statistical uncertainties (solid black line) and simulated line shapes (dashed red line) generated with $R_p = 0.85$ and $R_\sigma = 3.2$ for three lifetimes: $\tau = 0.50$ ps (a), $\tau = 2.14$ ps (b), and $\tau = 4.50$ ps (c). Background contributions are shown in gray. The data and simulated line shapes (0.50 ps, dotted blue line; 2.14 ps, dashed red line; and 4.50 ps, dashed blue line) are replotted for comparison (d) over the same energy range as the plots in Figs. 3(b)–3(d). The best-fit lifetime of 2.14 ps is taken from the minimum of the black curve for $R_p = 0.85$ in Fig. 5(c).

with those of the complementary technique presented in detail in Refs. [12,33,34]. There, a one-neutron knockout reaction of ^{20}Mg on a thick beryllium target at 450 MeV/nucleon was used to populate states in ^{19}Mg. The energy and angles of all three ^{19}Mg decay products were measured independently, and from the reconstructed decay vertex profile, a lifetime of $\tau = 5.8(22)$ ps was deduced. Prompt contributions to the decay vertex profile had to be accounted for as their impact on the lifetime analysis was identical to that of R_p on the present analysis. From the measured proton–^{17}Ne angular correlations, the authors determined the prompt contribution of the ^{17}Ne yield to be 89(1)% [35] from the analysis presented in Ref. [36].

With this value in mind, knockout-reaction cross section ratios were calculated using the proper beam energies and target compositions for the two measurements in order to restrict R_p for the present work. First, calculations of p-wave neutron removal from the ^{20}Mg secondary beam to the $1/2^-$ ground state and low-lying $3/2^-$ excited states in ^{19}Mg [36] were performed. The results indicated a modest 4% increase in both ^{19}Mg ground state production—the only source of delayed ^{17}Ne—and excited state production—one source of prompt ^{17}Ne—for our work compared to Ref. [12]. Next, multinucleon-removal calculations of the $2p1n$ breakup of ^{20}Mg to ^{17}Ne and the $1p1n$ breakup to ^{18}Na—both prompt processes producing ^{17}Ne—were performed. The calculations treated all valence nuclei as uncorrelated and equally available for removal and then computed the geometric probability that $2p1n$ or $1p1n$ groupings would be struck and removed by the target; this uncorrelated model is discussed briefly in Refs. [37,38]. The results indicated 7% less production of prompt ^{17}Ne from these channels in our work compared to Ref. [12]. From this information, we calculate $R_p = 0.87$ for our measurement. Attaching a conservative uncertainty of $\pm 5\%$, we arrive at the constrained range $R_p = [0.82, 0.92]$ and have investigated the best-fit lifetime at the additional values of 0.82, 0.88, 0.90, and 0.92.

Hence, simulated energy-loss line shapes were generated over a broad lifetime range for all R_p-R_σ pairs. A varying normalization factor accounted for statistical differences between the simulations and data. The 0.0 mm energy-loss data were found to be the most sensitive to lifetime effects due to the dominance of prompt ^{17}Ne production mechanisms along with the short ^{19}Mg lifetime. We have therefore only used these data for the full analysis. Distributions of χ^2 values from the fits of simulated and experimental spectra were constructed for each R_p-R_σ pair. The best-fit lifetimes and statistical errors ($\chi^2_{\min} + 1$) were taken from cubic polynomial fits to these distributions for R_p values in the range 0.05 to 0.90. The distributions obtained for $R_p = 0.92$ and 0.95 were quite broad and best fit with phenomenological power laws. Samples of nine such fits are provided in Fig. 5 for $R_p = 0.35$, 0.55, and 0.85 and all three R_σ values. The sensitivity to small changes in lifetime is enhanced for small values of R_p as expected; with limited contributions from prompt ^{17}Ne production processes, the intensity ratio of the small ^{19}Mg and prominent ^{17}Ne energy-loss peaks is heavily dependent upon the ground state $2p$-decay lifetime. Figure 6 illustrates the sensitivity of the simulated line-shape features to changes in lifetime. These simulations were generated using $R_p = 0.85$ and $R_\sigma = 3.2$. The superior fit of the $\tau = 2.14$ ps simulation is clear; this lifetime value was extracted from the minimum of the black curve in Fig. 5(c).

Figure 5 demonstrates that the spread in best-fit lifetimes introduced by the variation of R_σ is insignificant compared to that from the variation of R_p. Therefore for each R_p, the best-fit lifetime is taken from the central value $R_\sigma = 3.2$ and

TABLE I. ^{19}Mg ground state $2p$-decay lifetime (in ps) as a function of the ^{17}Ne production mechanism ratio R_p. The asymmetric error bars are due largely to the cubic polynomial fits to the distributions of χ^2 values in Fig. 5; there it is clear that the third-order term's coefficient becomes more significant at large R_p.

	R_p													
	0.05	0.15	0.25	0.35	0.45	0.55	0.65	0.75	0.82	0.85	0.88	0.90	0.92	0.95
τ	0.32	0.35	0.43	0.48	0.57	0.67	0.85	1.22	1.75	2.14	2.97	3.7	6.4	8.1
$\delta\tau_{\text{total}}$	$^{+0.11}_{-0.12}$	$^{+0.12}_{-0.12}$	$^{+0.14}_{-0.14}$	$^{+0.16}_{-0.15}$	$^{+0.18}_{-0.18}$	$^{+0.21}_{-0.21}$	$^{+0.25}_{-0.24}$	$^{+0.33}_{-0.32}$	$^{+0.43}_{-0.42}$	$^{+0.49}_{-0.52}$	$^{+0.68}_{-0.61}$	$^{+1.0}_{-1.3}$	$^{+2.4}_{-2.7}$	—

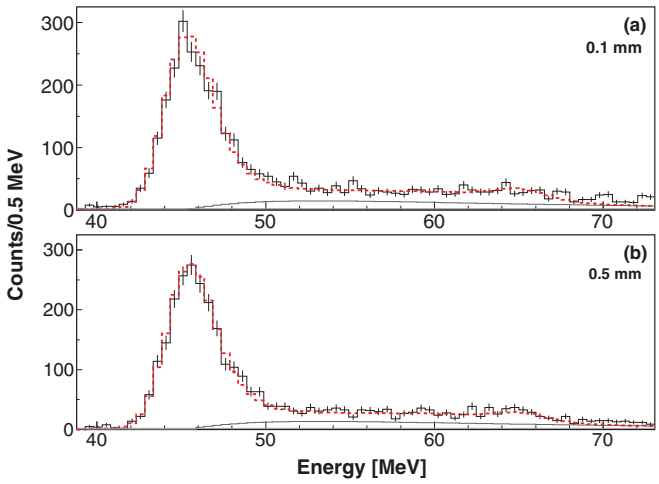

FIG. 7. (Color online) The 0.1 mm (a) and 0.5 mm (b) experimental DSSD spectra in coincidence with incoming ^{20}Mg on the target and outgoing ^{17}Ne in the S800 with statistical uncertainties (solid black line) and simulated line shapes (dashed red line) generated with $R_p = 0.85$ and $R_\sigma = 3.2$ for the best-fit lifetime of $\tau = 2.14$ ps extracted from fits to the 0.0 mm energy-loss data. Background contributions are shown in gray.

those from simulations of the upper and lower R_σ limits form the main contribution to the systematic error. Discrepancies between the experimental and the simulated reaction- and decay-residue momentum distributions affect energy losses and comprise a second source of uncertainty. The impact of this systematic error was investigated with small variations in both the target and detector thickness and the S800 momentum acceptance. These changes were found to contribute only half as much as the uncertainties of R_σ. The sum of these two systematic errors was adopted for the final results as all other sources were found to be negligible. Table I summarizes the best-fit lifetime results with the total systematic and statistical errors summed. No clear minimum was obtained for the distribution of χ^2 values at $R_p = 0.95$; the distribution flattened at 8.1 ps and this has been taken as a lower limit on the lifetime.

As a consistency check, the simulated energy losses for the best-fit lifetime of 2.14 ps at $R_p = 0.85$ and target-DSSD distances of 0.1 and 0.5 mm are plotted against the corresponding experimental DSSD spectra in Fig. 7. The compatibility in shape indicates that using the 0.0 mm energy-loss data for the full line-shape analysis did not bias the results. Figure 8 summarizes the best-fit lifetimes and total uncertainties in Table I to illustrate the lifetime trend as a function of increasing R_p. The literature value of $\tau = 5.8 \pm 2.2$ ps [12], for which R_p was quoted as 0.89 [35], is plotted as well. It agrees well with the present results of $2.97^{+0.68}_{-0.61}$ and $3.7^{+1.0}_{-1.3}$ ps at R_p values of 0.88 and 0.90, respectively. To account for the uncertainty in the ^{17}Ne production mechanism ratio R_p, which spanned values between 0.82 and 0.92 in the present data, we have adopted a broader range of lifetimes between $1.75^{+0.43}_{-0.42}$ and $6.4^{+2.4}_{-2.7}$ ps as the final result.

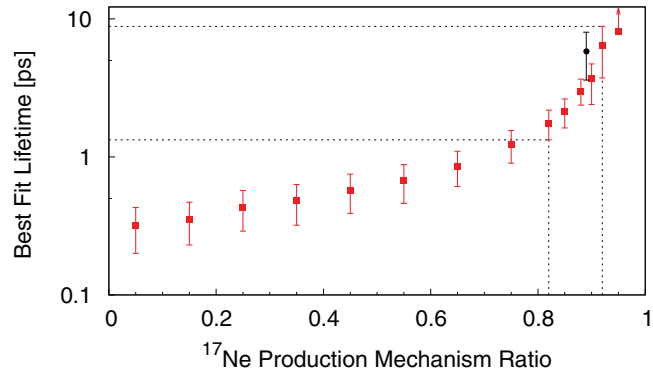

FIG. 8. (Color online) ^{19}Mg ground state $2p$-decay lifetime as a function of increasing ^{17}Ne prompt production (red squares) with statistical and systematic uncertainties summed. Dashed horizontal lines indicate the 1σ lower- and upper-limit best-fit lifetimes for the $R_p = 0.82$ and $R_p = 0.92$ bounds, respectively. The literature result (black circle) from Ref. [12] is plotted for comparison.

V. CONCLUSION AND OUTLOOK

In summary, we have developed an adaptation of the recoil distance method for lifetime studies of short-lived proton-emitting nuclei beyond the drip line. We report the results of the first application of this particle plunger technique that provides a complementary measurement of the ground state $2p$-decay lifetime of ^{19}Mg. A range of lifetimes was deduced as a function of the prompt contribution of the observed ^{17}Ne decay-residue yield. With guidance from the previous measurement and knockout-reaction cross section calculations, we have determined a range for the prompt ^{17}Ne contribution from 82% to 92%, corresponding to lifetimes between $1.75^{+0.43}_{-0.42}$ and $6.4^{+2.4}_{-2.7}$ ps, respectively. These results are consistent with the previously reported ^{19}Mg lifetime measurement and serve as an important validation of this new method for measuring lifetimes of exotic, short-lived proton emitters. Few direct experimental approaches for picosecond-ordered proton-emission lifetime measurements exist, thus the method introduced in this paper offers a valuable experimental addition. Future precision lifetime measurements with the technique introduced here, especially coupled with a simultaneous constraint of the prompt contribution to the yield of the $2p$-decay residue, would be of great interest.

ACKNOWLEDGMENTS

The authors gratefully acknowledge the support and expertise of the NSCL Coupled Cyclotron Facility, A1900, and computer staff for their assistance during the experiment and analysis. This work was supported in part by U.S. NSF Grant Nos. PHY-0606007 and PHY-1102511. P.V. and K.S. additionally acknowledge the support of the National Sciences and Engineering Research Council of Canada awards SAPIN/371656-2010 and SAPEQ/390539-2010 and the Simon Fraser University Vice President, Research. J.A.T. acknowledges support from the Science and Technology Facilities Council (UK) Grant No. ST/J000051.

[1] V. I. Goldansky, Nucl. Phys. **19**, 482 (1960).
[2] M. Pfützner *et al.*, Eur. Phys. J. A **14**, 279 (2002).
[3] J. Giovinazzo *et al.*, Phys. Rev. Lett. **89**, 102501 (2002).
[4] C. Dossat *et al.*, Phys. Rev. C **72**, 054315 (2005).
[5] K. Miernik *et al.*, Phys. Rev. Lett. **99**, 192501 (2007).
[6] M. Pomorski *et al.*, Phys. Rev. C **83**, 061303 (2011).
[7] B. Blank *et al.*, Phys. Rev. Lett. **94**, 232501 (2005).
[8] L. V. Grigorenko, R. C. Johnson, I. G. Mukha, I. J. Thompson, and M. V. Zhukov, Phys. Rev. Lett. **85**, 22 (2000).
[9] L. V. Grigorenko and M. V. Zhukov, Phys. Rev. C **68**, 054005 (2003).
[10] M. Pfützner *et al.*, Rev. Mod. Phys. **84**, 567 (2012).
[11] A. Dewald *et al.*, Prog. Part. Nucl. Phys. **67**, 786 (2012).
[12] I. Mukha *et al.*, Phys. Rev. Lett. **99**, 182501 (2007).
[13] L. V. Grigorenko *et al.*, Nucl. Phys. A **713**, 372 (2003).
[14] H. T. Fortune and R. Sherr, Phys. Rev. C **76**, 014313 (2007).
[15] H. T. Fortune and R. Sherr, Phys. Rev. C **83**, 057301 (2011).
[16] M. Assié *et al.*, Phys. Lett. B **712**, 198 (2012).
[17] A. Dewald *et al.*, GSI Scientific Report, GSI Report 2006-01, 38 (2005).
[18] D. Bazin *et al.*, Nucl. Instrum. Meth. B **204**, 629 (2003).
[19] D. J. Morrissey *et al.*, Nucl. Instr. Meth. B **204**, 90 (2003).
[20] J. Yurkon *et al.*, Nucl. Instrum. Meth. A **422**, 291 (1999).
[21] T. Zerguerras *et al.*, Eur. Phys. J. A **20**, 389 (2004).
[22] H. T. Fortune and R. Sherr, Phys. Rev. C **72**, 034304 (2005).
[23] S. Agostinelli *et al.*, Nucl. Instrum. Meth. A **506**, 250 (2003).
[24] R. Brun and F. Rademakers, Nucl. Instrum. Meth. A **389**, 81 (1997).
[25] P. Adrich *et al.*, Nucl. Instrum. Meth. A **598**, 454 (2009).
[26] M. Petri *et al.*, Phys. Rev. Lett. **107**, 102501 (2011).
[27] P. Voss *et al.*, Phys. Rev. C **86**, 011303(R) (2012).
[28] F. de Oliveira Santos *et al.*, Eur. Phys. J. A **24**, 237 (2005).
[29] K. Sümmerer and B. Blank, Phys. Rev. C **61**, 034607 (2000).
[30] O. B. Tarasov and D. Bazin, Nucl. Instrum. Meth. B **204**, 174 (2003).
[31] J.-J. Gaimard and K.-H. Schmidt, Nucl. Phys. A **531**, 709 (1991).
[32] O. B. Tarasov and D. Bazin, Nucl. Instrum. Meth. B **266**, 4657 (2008).
[33] I. Mukha *et al.*, Phys. Rev. C **77**, 061303(R) (2008).
[34] I. Mukha *et al.*, Phys. Rev. C **82**, 054315 (2010).
[35] I. Mukha, private communication (2013).
[36] I. Mukha *et al.*, Phys. Rev. C **85**, 044325 (2012).
[37] D. Bazin *et al.*, Phys. Rev. Lett. **91**, 012501 (2003).
[38] J. A. Tostevin, G. Podolyák, B. A. Brown, and P. G. Hansen, Phys. Rev. C **70**, 064602 (2004).